Runaway electron synchrotron radiation in a vertically translated plasma

M Hoppe[1], G Papp[2], T Wijkamp[3,4], A Perek[3], J Decker[5], B Duval[5], O Embreus[1], T Fülöp[1], U A Sheikh[5] the TCV Team[†] and the EUROfusion MST1 Team[*]

[1]Department of Physics, Chalmers University of Technology, SE-41296 Gothenburg, Sweden
[2]Max Planck Institute for Plasma Physics, D-85748 Garching, Germany
[3]FOM Institute DIFFER 'Dutch Institute for Fundamental Energy Research', 5600 HH Eindhoven, Netherlands
[4]Department of Applied Physics, Eindhoven University of Technology, Eindhoven 5600 MB, Netherlands
[5]Swiss Plasma Centre, EPFL, CH-1015 Lausanne, Switzerland
[†]See the author list of "S. Coda *et al.*, 2019 Nucl. Fusion **59** 112023"
[*]See the author list of "B. Labit *et al.*, 2019 Nucl. Fusion **59** 086020"

E-mail: `hoppe@chalmers.se`

February 2020

Abstract. Synchrotron radiation observed from runaway electrons (REs) in tokamaks depends upon the position and size of the RE beam, the RE energy and pitch distributions, as well as the location of the observer. We show experimental synchrotron images of a vertically moving runaway electron beam sweeping past the detector in the TCV tokamak and compare it with predictions from the synthetic synchrotron diagnostic Soft. This experimental validation lends confidence to the theory underlying the synthetic diagnostics which are used for benchmarking theoretical models of and probing runaway dynamics. We present a comparison of synchrotron measurements in TCV with predictions of kinetic theory for runaway dynamics in uniform magnetic fields. We find that to explain the detected synchrotron emission, significant non-collisional pitch angle scattering as well as radial transport of REs would be needed. Such effects could be caused by the presence of magnetic perturbations, which should be further investigated in future TCV experiments.

Submitted to: *Nucl. Fusion*

1. Introduction

One of the key issues facing future reactor-scale tokamaks, such as ITER, is plasma terminating disruptions. Such events can convert a significant part of the plasma current to relativistic runaway electron (RE) current. Uncontrolled loss of the RE current may then damage the plasma facing components and must be avoided. Therefore, in recent years, much effort has been devoted to developing strategies for preventing or mitigating the effect of REs [1–3]. Evaluating these strategies requires reliable theoretical models for RE generation and their subsequent dynamics. However, most theoretical and numerical models currently available to the community, and used e.g. in predictions for ITER, have yet to be thoroughly benchmarked against experimental data.

A powerful diagnostic method for REs within a plasma is to measure their *synchrotron radiation* [4]. The radiation spectrum emitted by the runaways, and the associated radiation spot observed in camera images, both depend on the momentum- and real-space distribution of the runaways. Synchrotron radiation measurements therefore provide insight into the pitch angle, energy [5, 6] and spatial distribution [7] of runaway electrons.

Measurements of synchrotron radiation emitted by REs have been performed on tokamaks since the early 90's [8, 9], with both visible-light/infrared spectrometers and cameras. During recent years, more advanced synthetic diagnostic tools have been developed [10, 11] that take into account the camera position and magnetic equilibrium. The application of synthetic synchrotron diagnostics to bridge the gap between theory and experiment is still under development, and the applicability of the synthetic diagnostics are not yet fully experimentally validated.

This letter reports a recent runaway electron experiment conducted at the Tokamak à Configuration Variable (TCV), situated at the Swiss Plasma Center in Lausanne, Switzerland. The highly elongated shape of the TCV chamber, combined with its rich set of poloidal field coils and sophisticated control software [12, 13], provides a unique opportunity to investigate the vertical dependence of synchrotron radiation emission. In TCV a high current conversion, fully developed runaway electron beam can be reliably displaced vertically over a distance comparable to the minor radius [12]. In the present experiment, a runaway electron beam was generated and maintained within an ohmically driven plasma in a non-disruptive phase. The circular, limited plasma is displaced vertically within the vacuum chamber, sweeping across the synchrotron camera's field-of-view and probing how the synchrotron spot depends upon the relative vertical position of the runaway beam and synchrotron detector. The experimental measurements show good qualitative agreement with the predictions obtained from the synthetic diagnostic tool Soft [11]. This experiment complements previous publications [6,7,14] by providing proof of the *vertical position* spot shape predictions from the synthetic synchrotron diagnostic.

2. Synchrotron radiation spot shapes

Synchrotron radiation is emitted primarily along the velocity vector of the emitting particle [15]. Synchrotron radiation, thus, is only observed when the emitting particle is moving directly towards the observer. In tokamak plasmas, synchrotron emission appears as asymmetric patterns of emissivity, the shape of which is sensitive to both the RE distribution function, as well as the detector position and magnetic field. The dependence of the synchrotron spot shape on these parameters has been extensively studied [10, 11, 16–18]. In this section, we restrict our attention to the emission shape dependence on the vertical distance ΔZ between the detector and runaway beam.

Often, the observed synchrotron spot depends sensitively only on a small subset of the runaway electron distribution function f_{RE}, namely where the product $\mathcal{P}(r,p,\theta) = G(r,p,\theta)f_{\mathrm{RE}}(r,p,\theta)$ attains a maximum. Here, $G(r,p,\theta)$ denotes the radiated power recorded by a given detector from an ensemble of electrons located on the same flux-surface labelled by r with the same momentum p and pitch angle θ in the point of minimum magnetic field along the orbit. If $\mathcal{P}$ is sharply peaked at the point $(p^\star,\theta^\star)$, the synchrotron spot will have nearly the same shape as if all particles had the same momentum and pitch angle

$$f_{\mathrm{RE}} \sim \delta(p-p^\star)\delta(\cos\theta-\cos\theta^\star). \tag{1}$$

It is therefore often possible to characterise synchrotron spots by the pair $(p^\star,\theta^\star)$ of parameters corresponding to the maximum of $\mathcal{P}$, i.e. the subset of runaway electrons that dominate synchrotron emission [19]. While this is most likely far from the true distribution of runaway electrons, this approximation matches experimental synchrotron measurements sufficiently well for the TCV discharge analysed in this letter. Other, physically motivated models for the distribution function were also considered for the TCV discharge, but for reasons to be discussed in section 3, these failed to predict the observed synchrotron radiation pattern. Therefore, in what follows, we will only consider synchrotron spots resulting from distribution functions of the form in equation (1).

To simulate the detected synchrotron radiation, we use the open source synthetic synchrotron diagnostic Soft [11]. Soft calculates the intensity of bremsstrahlung and/or synchrotron radiation reaching a given detector, in an arbitrary, axisymmetric

magnetic geometry. The guiding-center formulation used in SOFT ensures short simulation times, while accurately accounting for the magnetic geometry, orbit drifts and radiation spectrum dependence on geometrical and particle parameters.

The position of the synchrotron detector relative to the plasma strongly affects the observed radiation spectrum and spot shape and, in particular, the vertical detector placement can change the observed part of the distribution function, i.e. the values of $p^\star$ and $\theta^\star$. If the vertical offset ΔZ of the detector relative to the plasma is non-zero, then electrons located within a radius

$$r \lesssim \frac{\Delta Z - D\tan\theta}{1 + (D + \Delta Z \tan\theta)\iota/2\pi R_\mathrm{m}}, \tag{2}$$

are not observed, where ι is the rotational transform, R_m the tokamak major radius and D the distance between the detector and runaway beam, since the electron velocity vectors never intersect the detector aperture. This may alter the observed part of the distribution function, possibly favouring the observation of runaways with large pitch angles. In practice, however, a vertical detector offset most likely always has a limited effect on the observed part of the distribution, since the total synchrotron radiation emitted by a single particle scales as $\sim \sin^2\theta$, inherently favouring the detection of large pitch-angle particles. For TCV discharge #64614, equation (2) yields a threshold pitch angle $\tan\theta_\mathrm{th} \lesssim \Delta Z/D \sim 0.1$, meaning that particles with smaller pitch angles could be out of the camera view. Hence, if the pitch angle $\theta^\star$ of the dominant particles is close to or smaller than θ_th, one could see a significant dependence on ΔZ in the dominant parameters $p^\star$ and $\theta^\star$. Conversely, if $\theta^\star > \theta_\mathrm{th}$, the dependence on ΔZ is weak for both $p^\star$ and $\theta^\star$.

A potential benefit of multiple camera views at different vertical positions was pointed out in ref. [16]. There, it was shown, albeit in a simplified geometry, that it is not possible to differentiate between a synchrotron spot resulting from runaways with an intermediate ($\sin\theta \sim r_\mathrm{beam}/D$) against a large pitch angle ($\sin\theta \gtrsim r_\mathrm{beam}/D$) using a single synchrotron camera. Using two cameras situated at different vertical positions, this degeneracy can be broken, and a wider range of pitch angles may be differentiated.

This conclusion holds for a more advanced treatment, such as the SOFT simulations, although the reasons differ. With SOFT, it is still possible to differentiate between pitch angles due to the pitch angle dependence of the toroidal origin of the radiation. Synchrotron spots corresponding to smaller pitch angles, however, tend to have distinct bright areas, running along the upper and lower edges of the spot [19]. These disappear for sufficiently high pitch angles, but by using two cameras at different vertical positions, it should be possible to extend the range of pitch angles for which the bright areas can be observed. This would, in particular, be useful when studying the (horizontal) polarization of synchrotron radiation that further emphasises the bright areas of the synchrotron spot [14, 20]. The additional information gained from having two vertically offset cameras is in most cases limited, compared to other possible system upgrades (e.g. observing the radiation in multiple wavelength ranges, combining camera data with spectral measurements, or measuring the polarisation).

3. Observation of a vertically translated plasma

The elongated vacuum chamber cross-section of TCV, illustrated in figure 1, combined with excellent plasma control capabilities [12, 13], makes TCV an ideal tokamak for studying the dependence of the runaway electron synchrotron spot on the vertical distance between the camera and runaway beam, which has not been studied experimentally before. In the approximately 1 second long, quiescent flat-top of TCV discharge #64614 (a type of plasma which references [21, 22] describe the general characteristics of), summarised in figure 2, a population of runaway electrons was generated and subsequently translated vertically from $Z = 10.7\,\mathrm{cm}$ to $Z = -2.0\,\mathrm{cm}$ ($\sim 60\%$ of the plasma minor radius). Before displacing the plasma, the synchrotron spot was allowed to develop and reach an asymptotic shape. The ohmically-heated discharge, $I_\mathrm{p} = 200\,\mathrm{kA}$, circular, limited plasma had a toroidal magnetic field $B_\mathrm{T} = 1.43\,\mathrm{T}$, major radius $R_\mathrm{p} = 0.86\,\mathrm{m}$ and minor radius $a_\mathrm{p} = 0.21\,\mathrm{m}$. The core electron density was held constant at approximately $n_\mathrm{e} = 0.8 \times 10^{19}\,\mathrm{m}^{-3}$, and the core electron temperature at about $T_\mathrm{e} = 1\,\mathrm{keV}$. A constant edge loop voltage was applied, resulting in an estimated electric field of $E \approx 0.25\,\mathrm{V/m}$ at the plasma center ($E/E_\mathrm{c} \approx 30$, $E/E_\mathrm{D} \approx 6\%$, where E_c is the Connor-Hastie field [23] and E_D the Dreicer field [24]), enabling runaway generation. Visible images were recorded using the multispectral imaging system MultiCam that distributes incoming light over four channels with different narrowband filters using beamsplitters so channels have a nearly identical observation geometry. Camera and data processing specifications are the same as those for the MANTIS system [25]. Figure 3 shows a selection of undistorted MultiCam images of the evolution of the synchrotron spot through a narrowband filter centered at 640.6 nm with full-width at half maximum of 1.73 nm (this range is selected for the lack of strong line emission). The detector

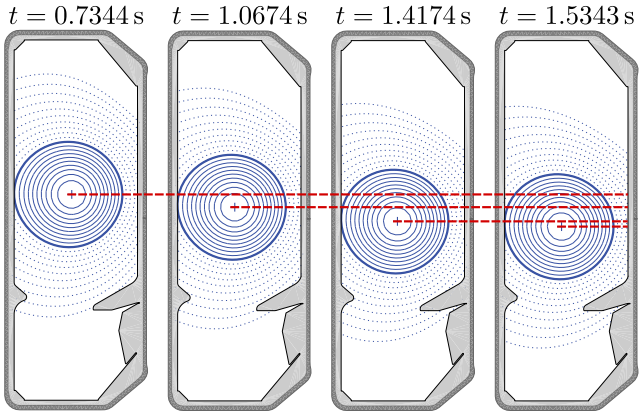

Figure 1. TCV plasma cross-section at approximately the four times considered in this letter. The plasma downward motion is indicated with the green dashed lines. The vertical magnetic axis location Z in these plasmas is, in order from earlier to later: $Z = 0.107\,\mathrm{m}$, $Z = 0.057\,\mathrm{m}$, $Z = -0.003\,\mathrm{m}$, and $Z = -0.020\,\mathrm{m}$.

Table 1. Parameters for the MultiCam detector used as input to Soft simulations.

Parameter	Value
Position (x, y, z)	$(1.082, -0.346, 0.014)\,\mathrm{m}$
Viewing direction	$(-0.794, -0.482, 0.054)$
Vision angle	$0.608\,\mathrm{rad}$
Camera roll	$0.023\,\mathrm{rad}$ (CCW)
Wavelength	$640.6\,\mathrm{nm}$

parameters used for the simulations are listed in table 1.

The synchrotron spot in discharge #64614 consists of two separate, oval parts—one large, vertically elongated and a smaller, horizontally elongated spot. As the plasma is translated vertically downwards, these two components correspondingly move downwards in the image, but at different rates. The smaller spot component (corresponding to runaways far from the detector) moves only slightly downwards, whereas the larger spot translates significantly during the scan.

The appearance of two distinct spots suggests that the dominant pitch angle is relatively large [11]. Using Soft simulations, we compare the contours of the simulated and experimental synchrotron images, and estimate the dominant particle parameters to be $\theta^\star \approx 0.40\,\mathrm{rad}$ and $p^\star \approx 50 m_e c$, where m_e is the electron rest mass and c the speed of light, so that $m_e c \approx 0.511\,\mathrm{MeV/c}$. We let the radial density profile of the REs take the form $n_{\mathrm{RE}}(r) \propto J_0(x_1 r/a_p)$, where $J_0(x)$ is a zeroth-order Bessel function of the first kind, and x_1 its first zero, which is the steady-state solution assuming a strong, diffusive radial transport with a uniform diffusion coefficient. The synchrotron patterns are most sensitive to variations in $\theta^\star$, and to support our estimate we present synthetic synchrotron images in the $t = 0.7344\,\mathrm{s}$ magnetic equilibrium for a few different values of $\theta^\star$ in figure 4. Comparing the images in figure 4 to figure 3a, we conclude that $\theta^\star = 0.4\,\mathrm{rad}$ is close to the lower limit for $\theta^\star$. At $\theta^\star = 0.6\,\mathrm{rad}$, the small synchrotron spot has begun to disappear behind the tokamak central column, allowing us to conclude that $\theta^\star = 0.6\,\mathrm{rad}$ is close to an upper limit for $\theta^\star$, as no part of the synchrotron pattern in figure 3a is obscured by the the tokamak wall. The synchrotron pattern is somewhat less sensitive to $p^\star$, but the RE energy influences the relative intensities of high-field side and low-field side emission [19], as well as the shift of the pattern due to orbit drifts. Based on these observations, we conclude that the dominant RE momentum should be near $p = 50 m_e c$.

Soft simulations for the vertical scan in TCV discharge #64614 are presented in figure 5. The synthetic images are generated for approximately the same times as figure 3. Soft requires magnetic equilibria at the desired times, and these were obtained from experimental measurements using the Grad-Shafranov magnetic reconstruction code Liuqe [26]. From the reconstructed equilibria, the relative distance between the plasma and camera port were calculated as (a) $\Delta Z = 9.3\,\mathrm{cm}$, (b) $\Delta Z = 4.3\,\mathrm{cm}$, (c) $\Delta Z = -1.7\,\mathrm{cm}$ and (d) $\Delta Z = -3.4\,\mathrm{cm}$, respectively, in figures 3 and 5.

The simulations in figure 5 exhibit the same dependence on ΔZ as the measurements in figure 3. As the plasma displaces down, the two parts of the synchrotron spot also move down. The smaller spot also appears to move more slowly than the larger spot, as described above. The underlying reason is the spatial origin of the radiation: the smaller spot originates from a position far from the detector, whereas the larger spot is located just in front of the detector, i.e. the different rates are due to the observer's perspective.

The runaway parameters inferred from synchrotron imaging can also be compared with predictions from conventional kinetic theory in axisymmetric magnetic fields. The superthermal infinite-aspect ratio electron kinetic equation is given by

$$\frac{\partial f}{\partial \nu_c t} + \frac{E_\parallel}{E_c}\frac{\partial f}{\partial q_\parallel} = \frac{1}{q^2}\frac{\partial \gamma^2 f}{\partial q} + \frac{1+Z_{\mathrm{eff}}}{2}\frac{\gamma}{q^3}\frac{\partial}{\partial \xi}\left[(1-\xi^2)\frac{\partial f}{\partial \xi}\right],$$

where $\xi = \cos\theta$, $q = p/m_e c$, $\gamma = \sqrt{1+q^2}$, Z_{eff} the ion effective charge and $\nu_c = 4\pi \ln\Lambda n_e c r_0^2$ with r_0 the classical electron radius, $\ln\Lambda$ the Coulomb logarithm. This kinetic equation makes three predictions that are contradicted by the synchrotron observations: (1) the primary (Dreicer) RE generation rate [23] at $E/E_D = 6\%$ and $Z_{\mathrm{eff}} = 1$ (assumed as no impurities were injected in this flat-top runaway scenario) corresponds to a RE current-generation rate $ec\partial n_{\mathrm{RE}}/\partial t \approx 1\,\mathrm{GAm^{-2}s^{-1}}$; (2) runaways with momentum $p \gg m_e c\sqrt{E_c/E} \approx 0.18 m_e c$ will be accelerated at a rate $\mathrm{d}p/\mathrm{d}t \approx eE_\parallel$ corresponding to

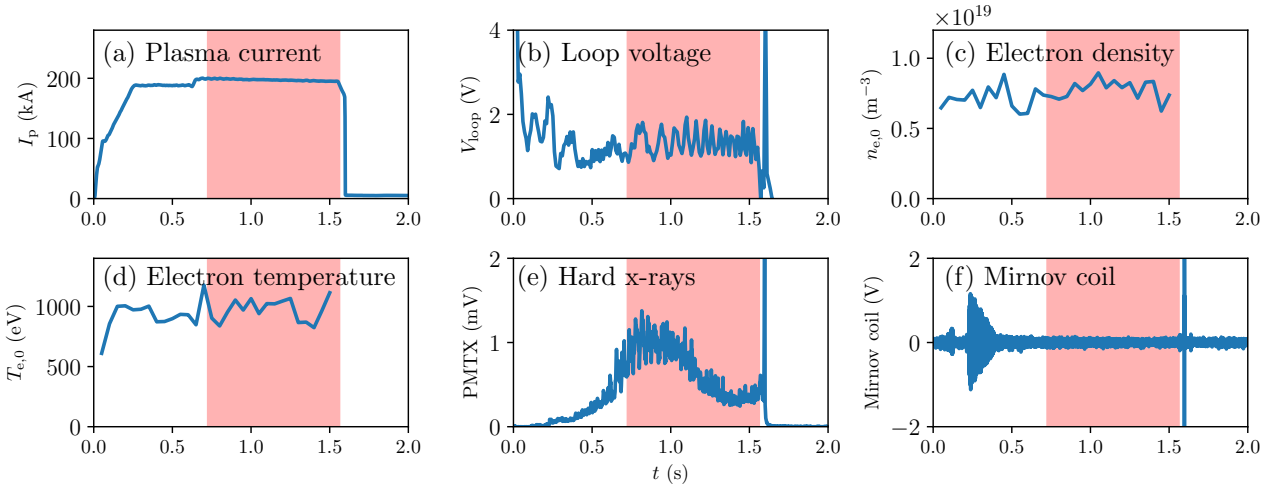

Figure 2. Time evolution of plasma parameters in TCV #64614. (a) plasma current, (b) loop voltage at plasma edge, (c) core electron density (from Thomson scattering), (d) core electron temperature (from Thomson scattering), (e) hard x-ray signal, (f) Mirnov coil signal. The timespan during which the plasma was vertically translated is indicated by the red shaded region.

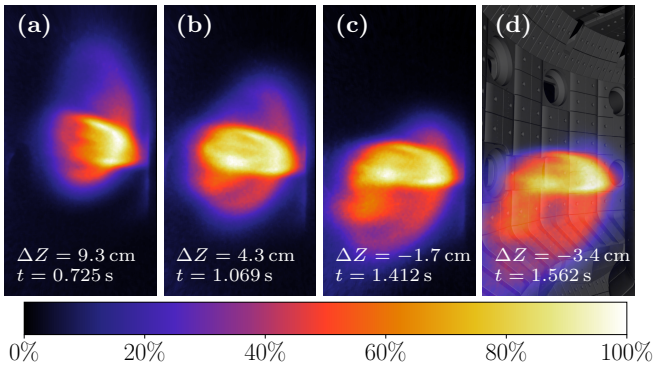

Figure 3. Synchrotron radiation images from the MultiCam camera system during TCV discharge #64614. The plasma is translated vertically downwards, past the camera, and the synchrotron spot changes accordingly. A CAD drawing of the camera view has been overlaid the image in (d). The two surfaces which make up the synchrotron spot can be distinguished and appear to be moving downwards at different rates. Note that in these images, the high-field side is to the right. Each pixel value indicates the received photon flux (photons/s), but due to that the camera was not absolutely calibrated, and in order to emphasize the radiation pattern, we normalize each frame to the value of its brightest pixel.

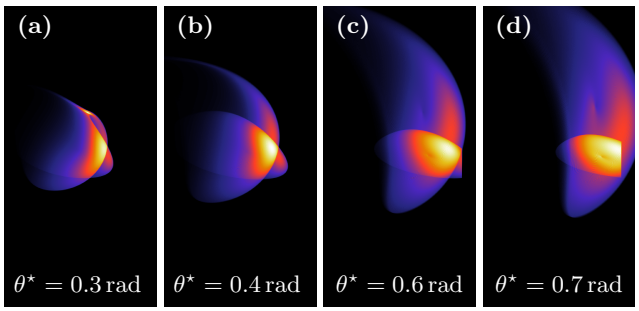

Figure 4. Synchrotron radiation images generated with Soft for a few different values of the dominant particle pitch angle $\theta^\star$ in the magnetic equilibrium at $t = 0.7344$ s. The dominant particle momentum is $p^\star = 50 m_e c$.

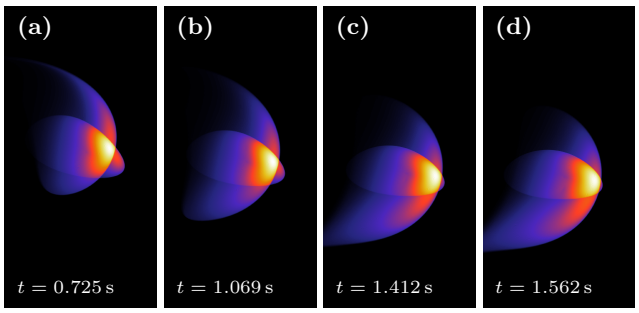

Figure 5. Synthetic synchrotron images generated with Soft with reconstructed plasma equilibria from TCV discharge #61614. In all simulations, $p^* = 50 m_e c$ and $\theta^* = 0.4$ rad.

a gain of $150\, m_e c$ per second—which due to significant Dreicer generation would lead to a corresponding increase of $p^\star$; (3) at relativistic speeds and small pitch angles, the runaway distribution takes the form [27] $f(t, p, \xi) = F(t, p)g(p, \xi)$ where the pitch-angle distribution g is independent of the evolving energy distribution F, and is given by $g \approx \exp[-A(1-\xi)]$ where $A = q(E/E_c)/(1+Z_{\text{eff}})$. The dominant emitting pitch can be estimated by weighing this pitch-angle distribution with the asymptotic synchrotron-emission formula in the high-frequency limit [28].

The result yields a maximum at $\theta \approx [(E/E_c)/(1+Z_{\text{eff}})]^{1/3} m_e c/p \approx 8 m_e c/p$ which would correspond to $\theta_\star \approx 0.16$ at $p_\star = 50\, m_e c$. These considerations together indicate that the axisymmetric kinetic

description is inadequate for describing the RE dynamics in TCV discharge #64614, a conclusion that holds true also if measurement errors are taken into account. A likely explanation is that magnetic perturbations play a significant role in the dynamics. Low-frequency perturbations can transport REs out of the plasma, which would suppress RE generation and maximum energies, whereas high-frequency (kinetic) instabilities may cause pitch-angle scattering [3, 29, 30] which could explain the anomalously high pitch angles. High-frequency kinetic instabilities have previously been invoked to explain discrepancies between idealized kinetic theory and experimental results under comparable plasma conditions in DIII-D [31].

Deviations in the appearance of the simulated synchrotron spots compared to the experimentally measured spots should mainly be due to (i) the particular choice (1) for the distribution function, (ii) errors in the estimated dominant particle $(p^\star, \theta^\star)$, (iii) errors in the calibrated detector and optical distortion model, and (iv) errors in the magnetic measurements used for reconstructing the plasma equilibrium. Error source (i) would primarily affect the distribution of intensity across the synchrotron spot, and if a full distribution function was used, it would give a more evenly distributed and smooth radiation pattern. Errors in the dominant particle (ii) primarily affect the size and overall (contour) shape of the spot, while an error in detector position (iii) is expected to only have a slight effect on the overall shape. Finally, errors in the plasma equilibrium (iv) may affect both the observed synchrotron spot position, its shape and the estimated dominant particle $(p^\star, \theta^\star)$. For (i) and (ii), a sensitivity scan has been conducted, concluding that the results presented here are robust, while for (iii) and (iv), estimates suggests that errors are negligibly small.

4. Conclusions

For the first time, the runaway electron synchrotron spot shape dependence on the vertical distance ΔZ between the runaway beam and the camera has been studied experimentally. It is found that the experimentally observed dependence qualitatively matches simulations conducted with the synthetic synchrotron diagnostic Soft well. These experiments therefore validate an important geometrical aspect of the theory underlying the synthetic diagnostic, and lend confidence to its capability of describing RE radiation in tokamaks. The multiple vertical views did however not provide sufficient additional information to more accurately constrain the runaway electron distribution function. This is primarily due to the large dominant pitch angle of the observed synchrotron spot, which allows the full vertical extent of the runaway beam to be observed regardless of the vertical position of the detector.

When comparing observations to predictions of conventional kinetic runaway theory, we find that kinetic theory significantly underestimate the observed dominant pitch angle $\theta^\star$ of the particles, while simultaneously greatly overestimating their energies. We hypothesise that the anomalously large dominant pitch angle observed could be due to the presence of kinetic instabilities, although no diagnostic was installed during the experiment to confirm this hypothesis. The runaway energies are most likely overestimated due to significant radial transport.

The ability of the MultiCam system to simultaneously obtain several images at different wavelengths was not utilised in this work, as it was not needed for the synthetic diagnostic validation. However, synchrotron radiation images at multiple wavelengths are expected to provide complementary information that can be used to further constrain the distribution function, and provide additional data points for validation of kinetic theory. This possibility will be explored in a future publication.

Acknowledgments

The authors gratefully acknowledge the help of A. Tema Biwole with retrieving plasma parameter signals. This work has been carried out within the framework of the EUROfusion Consortium and has received funding from the Euratom research and training programme 2014 - 2018 and 2019 - 2020 under grant agreement No 633053. This project has received funding from the European Research Council (ERC) under the European Union's Horizon 2020 research and innovation programme under grant agreement No 647121. The views and opinions expressed herein do not necessarily reflect those of the European Commission. The work was also supported by the Swedish Research Council (Dnr. 2018-03911) and the EUROfusion - Theory and Advanced Simulation Coordination (E-TASC).

References

[1] Lehnen M, Aleynikova K, Aleynikov P, Campbell D, Drewelow P, Eidietis N, Gasparyan Y, Granetz R, Gribov Y, Hartmann N, Hollmann E, Izzo V, Jachmich S, Kim S H, Kočan M, Koslowski H, Kovalenko D, Kruezi U, Loarte A, Maruyama S, Matthews G, Parks P, Pautasso G, Pitts R, Reux C, Riccardo V, Roccella R, Snipes J, Thornton A and de Vries P 2015 *Journal of Nuclear Materials* **463** 39 – 48 URL https://doi.org/10.1016/j.jnucmat.2014.10.075

[2] Hollmann E M, Aleynikov P B, Fülöp T, Humphreys D A, Izzo V A, Lehnen M, Lukash V E, Papp G, Pautasso G,

Saint-Laurent F and Snipes J A 2015 *Physics of Plasmas* **22** 021802 URL https://doi.org/10.1063/1.4901251

[3] Breizman B N, Aleynikov P, Hollmann E M and Lehnen M 2019 *Nuclear Fusion* **59** 083001 URL https://doi.org/10.1088/1741-4326/ab1822

[4] Jaspers R, Lopes Cardozo N J, Donné A J H, Widdershoven H L M and Finken K H 2001 *Review of Scientific Instruments* **72** 466–470 URL https://doi.org/10.1063/1.1318245

[5] Paz-Soldan C, Cooper C M, Aleynikov P, Eidietis N W, Lvovskiy A, Pace D C, Brennan D P, Hollmann E M, Liu C, Moyer R A and Shiraki D 2018 *Physics of Plasmas* **25** 056105 URL https://doi.org/10.1063/1.5024223

[6] Tinguely R, Granetz R, Hoppe M and Embréus O 2018 *Nuclear Fusion* **58** 076019 URL https://doi.org/10.1088/1741-4326/aac444

[7] Tinguely R A, Granetz R S, Hoppe M and Embréus O 2018 *Plasma Physics and Controlled Fusion* **60** 124001 URL https://doi.org/10.1088/1361-6587/aae6ba

[8] Finken K, Watkins J, Rusbüldt D, Corbett W, Dippel K, Goebel D and Moyer R 1990 *Nuclear Fusion* **30** 859 URL https://doi.org/10.1088/0029-5515/30/5/005

[9] Jaspers R, Grewe T, Finken K, Krämer-Flecken A, Cardozo N L, Mank G and Waidmann G 1995 *Journal of Nuclear Materials* **220-222** 682 – 687 ISSN 0022-3115 plasma-Surface Interactions in Controlled Fusion Devices URL https://doi.org/10.1016/0022-3115(94)00565-6

[10] Carbajal L and del Castillo-Negrete D 2017 *Plasma Physics and Controlled Fusion* **59** 124001 URL https://doi.org/10.1088/1361-6587/aa883e

[11] Hoppe M, Embréus O, Tinguely R, Granetz R, Stahl A and Fülöp T 2018 *Nuclear Fusion* **58** 026032 URL https://doi.org/10.1088/1741-4326/aa9abb

[12] Carnevale D, Ariola M, Artaserse G, Bagnato F, Bin W, Boncagni L, Bolzonella T, Bombarda F, Buratti P, Calacci L, Causa F, Coda S, Cordella F, Decker J, Tommasi G D, Duval B, Esposito B, Ferrò G, Ficker O, Gabellieri L, Gabrielli A, Galeani S, Galperti C, Garavaglia S, Havranek A, Gobbin M, Gospodarczyk M, Granucci G, Joffrin E, Lennholm M, Lier A, Macusova E, Martinelli F, Martìn-Solìs J R, Mlynar J, Panaccione L, Papp G, Passeri M, Pautasso G, Popovic Ž, Possieri C, Pucella G, Sheikh U A, Ramogida G, Reux C, Rimini F, Romano A, Sassano M, Tilia B, Tudisco O and Valcarcel D 2019 *Plasma Physics and Controlled Fusion* **61** 014036 URL https://doi.org/10.1088/1361-6587/aaef53

[13] Decker J *et al.* 2020 (in preparation)

[14] Tinguely R, Hoppe M, Granetz R, Mumgaard R and Scott S 2019 *Nuclear Fusion* **59** 096029 URL https://doi.org/10.1088/1741-4326/ab2d1d

[15] Schwinger J 1949 *Phys. Rev.* **75**(12) 1912–1925 URL https://doi.org/10.1103/PhysRev.75.1912

[16] Jaspers R 1995 *Relativistic runaway electrons in tokamak plasmas* Ph.D. thesis Technische Universiteit Eindhoven URL https://inis.iaea.org/search/search.aspx?orig_q=RN:27012481

[17] Pankratov I M 1996 *Plasma Physics Reports* **22** 535

[18] Zhou R J, Pankratov I M, Hu L Q, Xu M and Yang J H 2014 *Physics of Plasmas* **21** 063302 URL https://doi.org/10.1063/1.4881469

[19] Hoppe M, Embréus O, Paz-Soldan C, Moyer R and Fülöp T 2018 *Nuclear Fusion* **58** 082001 URL https://doi.org/10.1088/1741-4326/aaae15

[20] Hoppe M, Embréus O, Svensson P, Unnerfelt L and Fülöp T 2018 Simulations of bremsstrahlung and synchrotron radiation from runaway electrons *Proceedings of the 45th EPS Conference on Plasma Physics* o5.J603 URL http://ocs.ciemat.es/EPS2018PAP/pdf/O5.J603.pdf

[21] Paz-Soldan C, Eidietis N W, Granetz R, Hollmann E M, Moyer R A, Wesley J C, Zhang J, Austin M E, Crocker N A, Wingen A and Zhu Y 2014 *Physics of Plasmas* **21** 022514 URL https://doi.org/10.1063/1.4866912

[22] Esposito B, Boncagni L, Buratti P, Carnevale D, Causa F, Gospodarczyk M, Martin-Solis J, Popovic Z, Agostini M, Apruzzese G, Bin W, Cianfarani C, Angelis R D, Granucci G, Grosso A, Maddaluno G, Marocco D, Piergotti V, Pensa A, Podda S, Pucella G, Ramogida G, Rocchi G, Riva M, Sibio A, Sozzi C, Tilia B, Tudisco O and Valisa M 2017 *Plasma Physics and Controlled Fusion* **59** 014044 URL https://doi.org/10.1088/0741-3335/59/1/014044

[23] Connor J and Hastie R 1975 *Nuclear Fusion* **15** 415–424 URL https://doi.org/10.1088/0029-5515/15/3/007

[24] Dreicer H 1959 *Phys. Rev.* **115**(2) 238–249 URL https://doi.org/10.1103/PhysRev.115.238

[25] Perek A, Vijvers W A J, Andrebe Y, Classen I G J, Duval B P, Galperti C, Harrison J R, Linehan B L, Ravensbergen T, Verhaegh K and de Baar M R 2019 *Review of Scientific Instruments* **90** 123514 URL https://doi.org/10.1063/1.5115569

[26] Moret J M, Duval B, Le H, Coda S, Felici F and Reimerdes H 2015 *Fusion Engineering and Design* **91** 1 – 15 ISSN 0920-3796 URL https://doi.org/10.1016/j.fusengdes.2014.09.019

[27] Fülöp T, Pokol G, Helander P and Lisak M 2006 *Physics of Plasmas* **13** 062506 URL https://doi.org/10.1063/1.2208327

[28] Bekefi G 1966 *Radiation processes in plasmas* (New York: Wiley) ISBN 978-990-063710-3

[29] Aleynikov P and Breizman B 2015 *Nuclear Fusion* **55** 043014 URL https://doi.org/10.1088/0029-5515/55/4/043014

[30] Spong D A, Heidbrink W W, Paz-Soldan C, Du X D, Thome K E, Van Zeeland M A, Collins C, Lvovskiy A, Moyer R A, Austin M E, Brennan D P, Liu C, Jaeger E F and Lau C 2018 *Phys. Rev. Lett.* **120**(15) 155002 URL https://doi.org/10.1103/PhysRevLett.120.155002

[31] Liu C, Hirvijoki E, Fu G Y, Brennan D P, Bhattacharjee A and Paz-Soldan C 2018 *Phys. Rev. Lett.* **120**(26) 265001 URL https://doi.org/10.1103/PhysRevLett.120.265001